ACS Catalysis

pubs.acs.org/acscatalysis

Research Article

Selective Removal of Acid Sites in Mordenite Zeolite by Trimethylchlorosilane Silylation to Improve Dimethyl Ether Carbonylation Stability

Rongsheng Liu, Shu Zeng, Tantan Sun, Shutao Xu, Zhengxi Yu,* Yingxu Wei, and Zhongmin Liu*

Cite This: *ACS Catal.* 2022, 12, 4491−4500

Read Online

ACCESS | Metrics & More | Article Recommendations | Supporting Information

ABSTRACT: Catalysis research always pursues more efficient catalysts and realizes selectivity-controlled conversion. The local environment of acid sites in a zeolite is regarded as the vital reason for its catalytic selectivity in many chemical reactions. Herein, we have demonstrated that the acid sites in the 12-membered-ring (12-MR) channels of mordenite zeolite could be selectively covered by a trimethylchlorosilane (TMCS) silylation treatment, which could significantly improve the dimethyl ether (DME) carbonylation performance. Detailed mechanism studies by *in situ* DRIFT, ^{1}H MAS NMR, and FTIR spectra analyses indicate that the TMCS species replace the Brønsted H^{+} in the bridging hydroxyl groups when chloro groups are rapidly hydrolyzed by the protons, accompanied by the formation of siloxane bonds. Due to the space limitation, the silylation reaction mainly occurred in the 12-MR channels and created most of the remaining acid sites (80%) in the 8-MR channels of the MOR zeolite, which gave better selectivity and a much longer lifetime in the DME carbonylation reaction. This work realizes a conceptual pathway to selectively control the distribution of acid sites within different confinement positions of zeolites to improve the catalytic selectivity of catalysts.

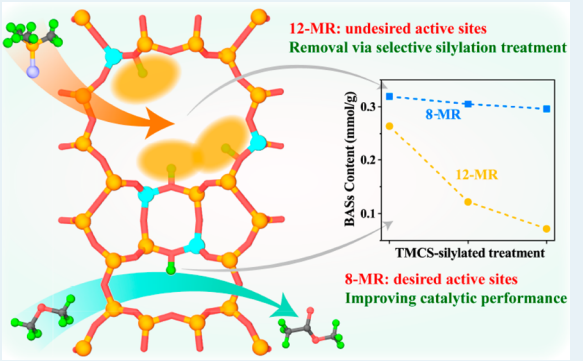

KEYWORDS: *mordenite, silylation treatment, acid distribution, DME carbonylation, catalytic stability, zeolite*

INTRODUCTION

Zeolites are widely employed as shape-selective catalysts that can minimize the use of raw materials and the formation of byproducts in many chemical processes.[1,2] The excellent catalytic performance of zeolites is usually attributed to the location of catalytically active sites, Brønsted acid sites (BASs), which are associated with protons compensating the negative charge generated by the presence of framework Al in the tetrahedral T sites.[3,4] The well-controlled local environment of BASs can restrict the formation of undesired products by adjusting the reactant or product diffusion and stabilizing the transition states and/or reaction intermediates for the desired reactions.[5,6] Hence, in the pursuit of unique reaction selectivity, it is expected that the targeted reaction will be performed at a specific position among all possible ones existing in a zeolite.

Mordenite (MOR) zeolite consists of both parallel 12-membered-ring (12-MR) (7.0 × 6.7 Å) and 8-MR (5.7 × 2.6 Å) channels, connected by 8-MR openings (4.8 × 3.4 Å) known as side pockets.[7,8] The BASs at different positions show distinct confinement effects for reactant molecules, especially reflected in a MOR zeolite catalyzing a dimethyl ether (DME) carbonylation reaction, which is a key step in converting syngas to ethanol.[9−11] It has been demonstrated that the 8-MR channels are preferred for the selective carbonylation of DME, where the local environment of BASs could stabilize the transition state involved in CO inserting into the bonded methyl group.[12−15] Corma et al. proposed from theoretical studies that the T3-O33 site in the 8-MR channel is the only position selective for carbonylation.[14] In contrast, as the larger 12-MR channels could accommodate more reaction routes, such as DME to hydrocarbons via a hydrocarbon pool (HCP) mechanism, a further HCP transformation to a coke reaction, etc., and the 12-MR channels provide transport channels for the reactions; the BASs in the 12-MR channel will cause rapid deactivation of the MOR zeolite.[15−19] Therefore, it is necessary to selectively remove the BASs in 12-MR channels and to control the BASs preferentially located in 8-MR channels of MOR to improve its catalytic performance in the DME carbonylation reaction.

Hitherto, many researchers have established various ways to tailor the acid site distribution of MOR zeolites. For instance,

Received: December 21, 2021
Revised: February 6, 2022

https://doi.org/10.1021/acscatal.1c05896
ACS Catal. 2022, 12, 4491−4500

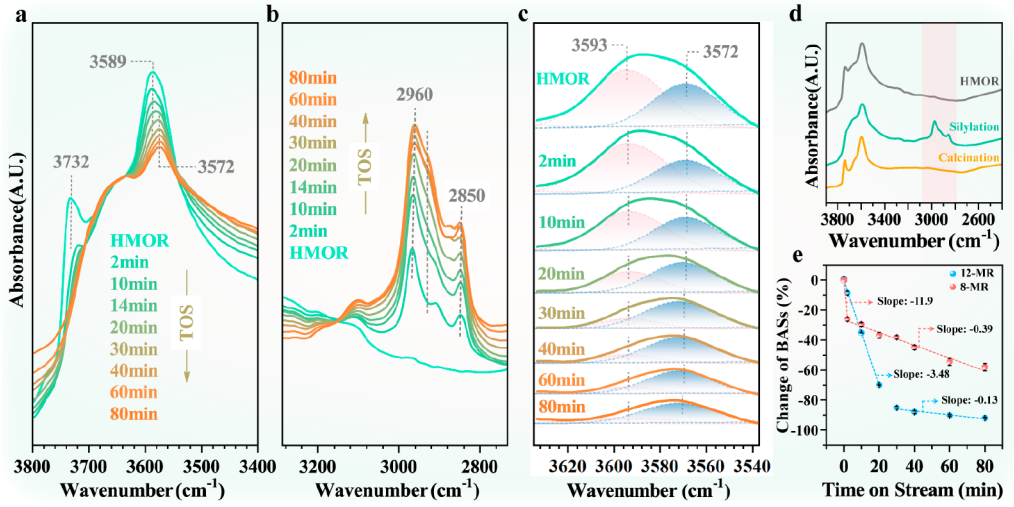

Figure 1. *In situ* DRIFT profiles of the silylation reaction of TMCS on HMOR with TOS at 450 °C: (a) O−H stretching region (3800−3400 cm^{-1}); (b) C−H stretching region (3000−2800 cm^{-1}); (c) deconvolution of the bridging O−H stretching region. The spectra were collected continuously after the TMCS molecules accessed HMOR zeolites at 450 °C. (d) DRIFT spectra of HMOR and silylated samples and the FTIR spectrum of this sample after calcination in the air at 550 °C for 6 h. (e) Change of BASs in different channels with TOS, the data obtained for BASs content acquired from the deconvoluted areas of Figure 1c.

new synthetic methods using different organic structure-directing agents (OSDAs) and introducing heteroatoms into the framework were established.[10,20,21] Postsynthesis treatments, such as steam[22] and alkaline/acid media[23,24] treatment, organic base modification,[25−27] etc., have also been studied for selective removal of the undesired acid sites within the 12-MR channels of MOR zeolites. Pyridine adsorption is the most effective method, since the stability of pyridine-adsorbed catalysts in the DME carbonylation reaction is distinctly superior to those prepared by other methods.[27,28] However, pyridine desorption often occurs under the reaction conditions, resulting in a gradual loss of activity by coke deposition.[22] Furthermore, the pyridine-adsorbed catalysts encounter challenges in their regenerability, in which calcination in air is usually employed to treat the deactivated catalysts, and preadsorption of pyridine was conducted again after regeneration. Given this, subsequent approaches, aimed at obtaining more efficient and lower-cost MOR zeolites for the DME carbonylation reaction, should address the questions mentioned above.

Another alternative approach to selectively control BAS distribution is by a silylation treatment of the zeolites. Silylation to preferentially cap the acid sites on the external surface of zeolites has been investigated extensively.[29−34] It may also be an effective approach to deactivate acid sites within the channels of zeolites when silylated agents are introduced into the internal surface of zeolites. McAteer and Rooney initially reported in 1973 that treatment with methylsilane allows modification of the acidity of the internal surface of HY zeolite.[35] Next, Barrer et al. investigated the silylation reaction of silane (SiH_4) in channels of the MOR zeolite and its sorption behaviors, without acidic and catalytic property results.[36,37] To obtain the desired distribution of acid sites for the DME carbonylation reaction, we tried to probe whether the acid sites in 12-MR channels of MOR can be selectively removed via a silylation method by introducing the silylated agent selectively and efficiently into the 12-MR rather than the 8-MR channels of MOR, which may be achieved in principle if the kinetic diameter of the chosen silylation agent is between the size of the 12-MR and the side pocket channels. The diffusion resistance imposed by the one-dimensional 12-MR channels should also be considered in selecting an agent to avoid a nonuniform internal silylation. It is expected that the side chain of the silylated agent can be decomposed during silylation to solve the problem. After many attempts with different silylation agents, trimethylchlorosilane (TMCS) (6.9 Å) was selected as a suitable silylation probe to selectively bond the Brønsted H^+ atoms within the 12-MR channels of MOR zeolites (Scheme S1).

Herein, we propose a facile approach for purposefully tailoring the acid site distribution via selective silylation and further elaborate the silylation reaction between TMCS molecules and acid sites in different positions and channels of MOR zeolites in a vapor-phase flow system. The TMCS-silylated zeolites are examined for their distribution and capacity of BASs in comparison to the untreated zeolite by various techniques and sensitive catalytic test reactions. The results indicate that this well-designed silylation method could selectively cover most of the undesired acid sites within 12-MR channels and ca. 80% of the remaining acid sites could be in the 8-MR environment of MOR zeolites. This BAS distribution significantly improves the catalytic selectivity and reaction stability of the MOR zeolites in the DME carbonylation to methyl acetate (MA) reaction.

RESULTS AND DISCUSSION

***In Situ* Insight into the Silylation Reaction of TMCS on HMOR.** First, we focus on the change of hydroxyl groups of HMOR zeolites, which are responsible for reacting with the TMCS molecules in the silylation reaction.[38,39] *In situ* DRIFT spectra were employed to investigate the silylation reaction of TMCS on HMOR and provided an entire picture of the variation trend of hydroxyl groups. Note that the IR band of OH groups gradually shifts in the peak-top position to lower frequencies and decreases in integrated intensity when the zeolites are heated at a higher temperature.[40] Figure 1 shows the *in situ* DRIFT spectra of the silylation reaction of TMCS on HMOR with time on stream (TOS) at 450 °C. The bands

https://doi.org/10.1021/acscatal.1c05896
ACS Catal. 2022, 12, 4491−4500

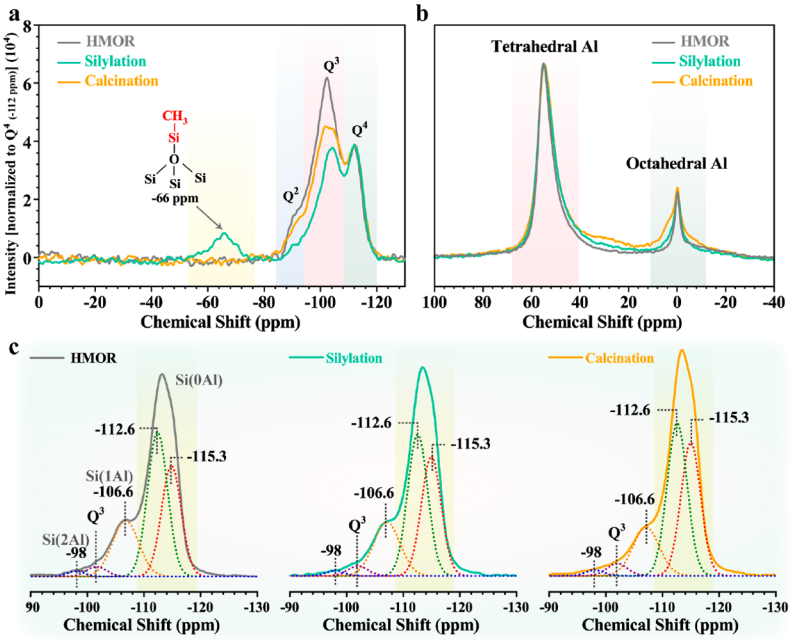

Figure 2. (a) $^{1}H-^{29}Si$ cross-polarization (CP), (b) ^{27}Al, and (c) ^{29}Si MAS NMR spectra of the untreated HMOR, TMCS-silylation HMOR at 450 °C, and this silylated HMOR zeolite after calcination in the air at 550 °C for 6 h.

at 3732 cm^{-1}, associated with the O−H stretching vibration of terminal Si−OH groups,[41] exhibited an overall declining trend and shifted toward a lower wavenumber with TOS (Figure 1a). This indicated that the terminal Si−OH groups could bond with TMCS molecules during the silylation reaction, consistent with previous studies.[38,42]

Another important observation of the HMOR samples during the silylation reaction is the appearance of vibration signals in the 3000−2800 cm^{-1} region (Figure 1b), which is usually the C−H stretching vibration region. These signals, related to the C−H bands of TMCS attached onto HMOR samples, can be divided into methyl, symmetric methylene, and antisymmetric methylene, respectively.[43,44] However, TMCS species attached on the HMOR sample only showed a single signal corresponding to methyl groups. These C−H stretching signals that appeared at 3000−2800 cm^{-1} might be attributed to the side products of methyl groups. At such high temperatures and feeding, the reaction between the methyl group as opposed to the chloro group in HMOR cannot be ruled out demonstrably, resulting in the further formation of the hydrocarbon species reflected by the bands at 3000−2800 cm^{-1}.[42] These C−H bands disappeared in the TMCS-silylated samples after calcination in the air (Figure 1d).

The most striking difference of HMOR zeolites duringthe silylation reaction was observed for the most important hydroxyl bands in the Si−OH−Al regions relevant to the catalytically active sites, which are actually composite bands comprised of high-frequency (HF) and low-frequency (LF) components at 3593 and 3572 cm^{-1}. They are related to stretching vibrations of the bridging hydroxyl groups within the 12-MR and 8-MR channels, respectively.[12,45] As shown in Figure 1a, the bridging O−H bands shifted to lower frequency and became more symmetrical with TOS, due to a preferential weakening of the HF band as TMCS bonded with HMOR zeolites. The detailed deconvoluted area ratios corresponding to BASs within 12-MR and 8-MR are given in Figure 1c,e. In the initial stage of the silylation reaction, about 2 min, both 12-MR and 8-MR BASs were reduced rapidly. Then 12-MR BASs were continuously and quickly decreased (slope of the change curve: −3.48) until about 30 min, at which time there appeared to be a maximum accessibility loss; beyond 30 min, they only showed a slightly reduced trend (slope of the change curve: −0.129). On the other hand, after 2 min, the 8-MR BASs remained slowly reduced (slope of the change curve: −0.391) with TOS. It can be seen that most of the TMCS molecules preferentially deposit in the 12-MR channels as opposed to the 8-MR channels of HMOR to bond with the BASs in channels. However, the remarkable thing is that the BASs within 8-MR environments also decreased during the silylation reaction. However, due to the restriction of the molecular size, TMCS molecules (6.9 Å) may not penetrate the 8-MR channels of HMOR zeolites to bond with the BASs. A possible explanation for this phenomenon is that the BASs in 8-MR channels are accessed and chemisorbed by the methyl groups and light hydrocarbon species formed during the silylation reaction. This hypothesis is verified by almost no loss of BASs in 8-MR channels after calcination, as shown in Figure 4. Therefore, we can conclude that this proposed treatment could remove the BASs selectively within 12-MR channels of HMOR zeolites by bonding with TMCS molecules.

The combination of an online mass spectrometer (MS) (Figure S1) and gas chromatograph (GC) (Figure S2) was employed to monitor the silylation reaction products continuously at different temperatures. During the silylation reaction, the main components of the outlet gas are HCl, methane, and unreacted TMCS (Figure S1a). Figure S1b shows that a higher temperature is beneficial to the evolution of methyl groups, but more HCl is produced at 450 °C (Figure S1c), which may be the optimal temperature for TMCS bonding with acid sites within HMOR. The GC studies suggest that ethylene, ethane, etc., are also released during the silylation reaction (Figure S2). On the basis of these analyses and the known reaction between the methyl groups with a chlorine group (or residual water) to give chloromethane (or

https://doi.org/10.1021/acscatal.1c05896
ACS Catal. 2022, 12, 4491−4500

Scheme 1. Schematic Depiction of a Typical Silylation Process, Showing Enriched BASs in the 8-MR Channels of HMOR Zeolite via a Selective TMCS-Silylation Treatment: (a) Silylation Reaction at the External Surface of HMOR Zeolite; (b) Silylation Reaction in the Internal Channels of HMOR Zeolite

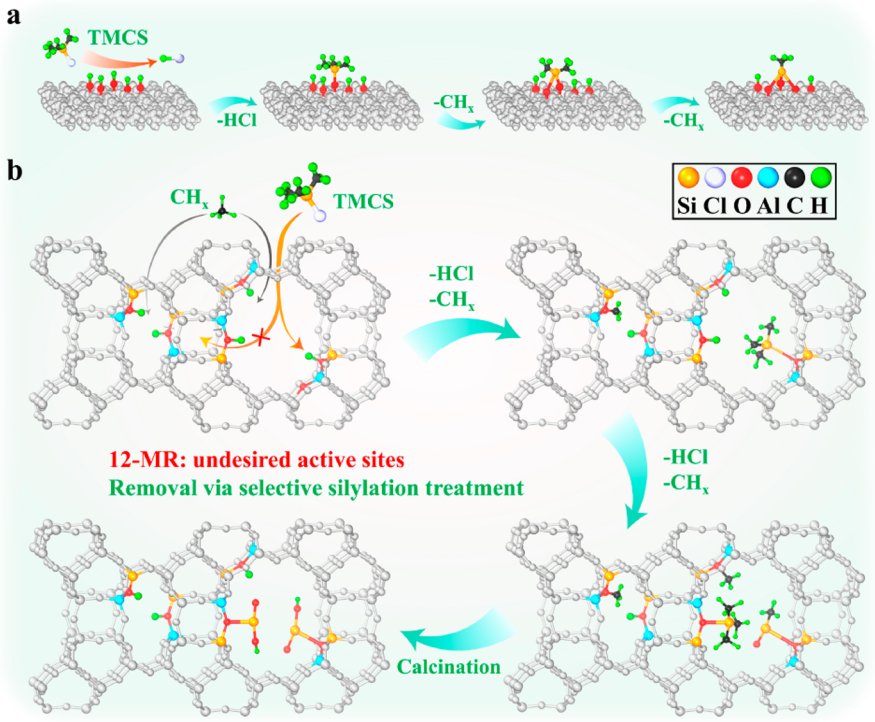

methanol), we can conclude that the silylation reaction is accompanied by chloromethane and/or methanol to hydrocarbons side reactions,[46−48] consistent with the *in situ* DRIFT results that showed the complicated C−H stretching bands. From the photos of all HMOR zeolites after the silylation reaction (Figure S3), coke formation was clearly seen on the surface of the treated zeolites. This is another indication that the side reaction occurred during the silylation reaction. Unfortunately, these hydrocarbon species and TMCS molecules adsorb competitively at the BASs that are responsible for TMCS bonding, which is disadvantageous to the level and efficiency of the removal of acid sites via a TMCS-silylation treatment.

Evolution of TMCS Species Anchored on HMOR. We have efficiently identified the TMCS functional groups anchored on the framework of HMOR zeolites during the silylation reaction by ^{1}H−^{29}Si cross-polarization (CP) NMR. Figure 2a shows the ^{29}Si CP NMR spectra of the untreated HMOR and the TMCS-silylated HMOR (450 °C) before and after calcination in air at 550 °C for 6 h, respectively. The resonance signals at −102 ppm in the three samples can be assigned to the Q^3, Si(OH)$(OSi)_3$, species. It is worth noting that the resonance peaks are also contributed by the presence of framework Al species (Si/Al = 16), corresponding to a neighboring signal at −106 ppm. The neighboring Q^4 signals at −112 ppm are related to $Si(OSi)_4$ units, originating from Si fully surrounded by other Si atoms. Moreover, a signal at −92 ppm can also be seen, assigned to the Q^2 species, $Si(OH)_2(OSi)_2$.[49,50] After the reaction with TMCS, the intensities of Q^3 and Q^2 resonance signals obviously decreased, indicating that the silanol groups could bond with TMCS molecules during the silylation reaction. Simultaneously, a newly appearing peak at −66 ppm of the NMR spectrum was observed, which might be related to tertiary silylation products ($MeSi(OSi)_3$), on the basis of a previous study.[38,51,52] The possible steps in the formation of tertiary methyltrisiloxysilanes are depicted in Scheme S1. Through the primary and secondary products, the TMCS species gradually react with three hydroxyl groups with concomitant evolution of HCl and a methyl group.[51] Unfortunately, we did not observe the primary and secondary products on silylated samples due to the higher silylation temperature. Moreover, after TMCS reacts with Si−OH−Al, Si−C bonds are broken at elevated temperature, splitting off methyl groups, and more highly substituted siloxane species are anchored to the framework.[52] After calcination, the newly appearing signal peak at −66 ppm faded away. Simultaneously, the Q^2 and Q^3 peaks increased significantly, indicating that the anchored TMCS functional groups transformed into new silanol groups (Si−OH) after calcination in air.

The thermal stability of the adsorbed TMCS species on HMOR samples was tested by a thermogravimetric analysis (TGA) combined with an online MS. A continuous mass loss was attributed to the desorption of water before 200 °C; after 200 °C, only a negligible mass loss was associated with the decomposition of the adsorbed TMCS species (Figure S4). According to the trend of MS, only m/z 15 corresponding to the methyl group was observed. Conversely, the amount of m/z 73 ($(CH_3)_3Si$) was almost negligible. Thus, it has been demonstrated that the methyl groups can be decomposed from the Si−C bond of TMCS species breaking with the elevated temperature, consistent with the presence of tertiary silylation products ($MeSi(OSi)_3$) as determined by ^{29}Si CP NMR spectra. The TMCS species bond stably with HMOR zeolites under all silylation conditions and the conditions chosen for property testing.

https://doi.org/10.1021/acscatal.1c05896
ACS Catal. 2022, 12, 4491−4500

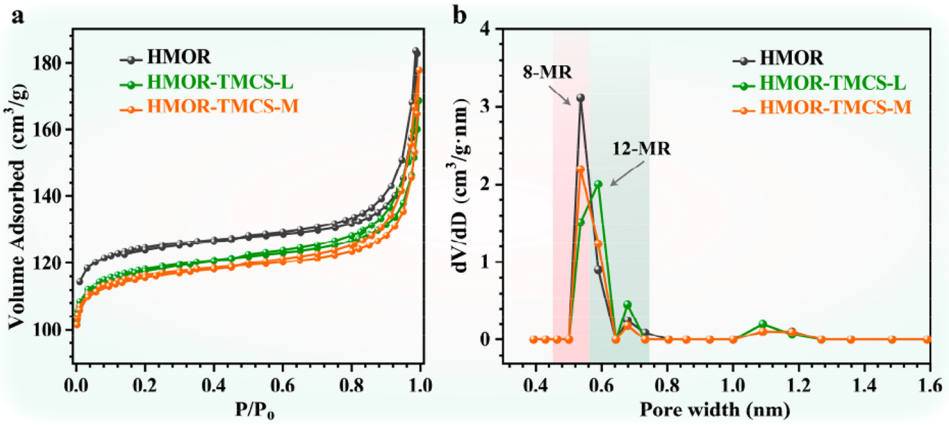

Figure 3. (a) N_2 sorption isotherms and (b) pore width distributions of the untreated and various TMCS-silylated HMOR zeolites.

To further trace the effect of the TMCS-silylation treatment on the framework of HMOR zeolites, ^{27}Al and ^{29}Si MAS NMR spectra were obtained, and the corresponding spectra of the untreated HMOR, the TMCS-silylated HMOR at 450 °C, and this silylated HMOR zeolite after calcination in the air at 550 °C for 6 h are given in Figure 2b,c, respectively. The ^{27}Al MAS NMR spectra show two apparent signals at 57 and 0 ppm, associated with the tetrahedrally coordinated and octahedrally coordinated Al species, respectively.[22,53] After silylation, the percentage of octahedrally coordinated Al increases from 14.1% to 15.2% in comparison to the untreated HMOR, indicating that a small fraction of Al is removed from the zeolite framework, which may be caused by the interaction with HCl that formed during the silylation reaction. In comparison, up to 18.5% of Al adopts an octahedral coordination after calcination in air at 550 °C for 6 h, due to the further removal of framework Al, which often occurs in zeolites during a thermal treatment.[54]

The broad peaks from −90 to −120 ppm of ^{29}Si MAS NMR spectra can be divided into four types of signals related to Si(2Al) (−98 ppm), Q^3 (−102 ppm), Si(1Al) (−106.6 ppm), and Si(0Al) (−112.6 and −115.3 ppm), respectively (Figure 2c).[24,55] Therefore, deconvolution was used to calculate the proportion of each signal, and the corresponding results are shown in Table S1. After reaction with TMCS, the intensity of the Si(1Al) and Si(2Al) resonance signals slightly decreases and the framework Si/Al ratio also increases from 16.2 to 17.1 correspondingly. Furthermore, the framework Si/Al ratio increases to 19.0 after calcination. This is consistent with the ^{27}Al MAS NMR result that a fraction of the framework Al adopts an octahedral coordination during the silylation treatment, and the removal of framework Al is mainly caused by the calcination after silylation.

The above physicochemical analyses of materials give an entire picture of the evolution of TMCS molecules bonding on HMOR zeolites and the change in the distribution of acid sites for materials during the TMCS-silylation reaction, to further infer the silylation reaction networks along with time on stream (Scheme 1). TMCS molecules first spread to the external surface of HMOR and gradually bond with three neighboring terminal Si−OH groups via a hydrolysis reaction accompanied by the formation of tertiary silylation products ($MeSi(OSi)_3$) and the release of methyl groups and HCl. Next, TMCS molecules diffuse into the channels of HMOR to react with the BASs within the internal channels. Due to the restriction of molecular size, TMCS (6.9 Å) only accesses 12-MR channels and replaces the Brønsted H^+ atoms via hydrolysis with the chloro groups. Then, the Si−C bonds are broken at elevated temperatures, splitting off methyl groups, leaving trisubstituted methyltrisiloxysilanes anchored onto the HMOR framework. The decomposition of methyl groups is beneficial to avoid hindering the back TMCS to enter into 12-MR channels. Methyl groups and HCl produced during the TMCS-silylation treatment further interreact through the intermediate products to give hydrocarbons, adsorbed competitively with TMCS on the BASs. These hydrocarbon species can also access 8-MR channels and bond with BASs here. Finally, the adsorbed hydrocarbon species are removed, and the anchored TMCS functional groups are transformed into new Si−OH groups after calcination in air.

Structural and Compositional Analyses. We prepared two representative samples with different treatment times at 450 °C (Figure S5) to test the effect on the physicochemical properties and catalytic performances in compariso to the parent HMOR materials. Combined techniques were employed to characterize the TMCS-silylated HMOR materials for their structure and composition. First, Figure S6 shows the XRD profiles of the parent and TMCS-silylated HMOR samples. All samples appear to the typical diffraction peaks of an MOR-like type. On the basis of the data, no shifts in the positions of diffraction peaks of all zeolites are observed after the silylation treatment, indicating that this modified treatment hardly changes the unit cell size of HMOR zeolites. The scanning electron microscopy (SEM) images show that the surface morphologies of the parent and TMCS-silylated HMOR samples are generally identical (Figure S7). Moreover, all HMOR zeolites exhibit a blocklike morphology with a size of about 200 nm and a significantly smooth surface, revealing that the silylation treatment has no effect on the crystalline structure of the HMOR samples, consistent with XRD results.

The specific surface areas and pore size distributions on the untreated and TMCS-silylate HMOR samples were determined by an N_2 adsorption−desorption experiment, which gives further evidence for the change in the structure of HMOR zeolites after the silylation treatment. The N_2 sorption isotherms and pore width distributions of all samples are given in Figure 3, and the corresponding data are given in Table S2. As shown in Figure 3a, the N_2 adsorption−desorption data are roughly similar. Additionally, the BET surface areas show an overall slight drop with increasing silylation time, and the

https://doi.org/10.1021/acscatal.1c05896
ACS Catal. 2022, 12, 4491−4500

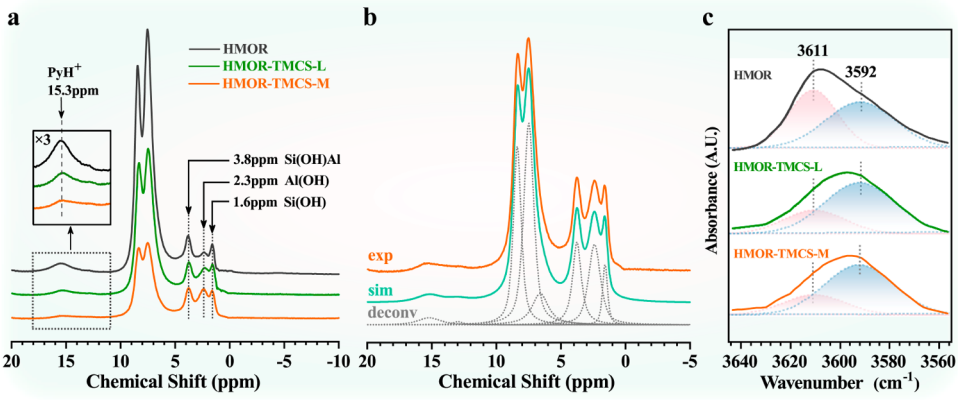

Figure 4. (a) ^{1}H MAS NMR spectra of the untreated and TMCS-silylated HMOR zeolites, (b) Deconvolution of ^{1}H MAS NMR spectra of HMOR-TMCS-M using DMFIT software. (c) FTIR spectra of the untreated and TMCS-silylated HMOR zeolites and deconvolutions in the 3660−3560 cm^{-1} region.

Table 1. Distribution and Capacity of the BASs of HMOR Zeolites Calculated on the Basis of the ^{1}H MAS NMR and FTIR

	^{1}H MAS NMR (mmol/g)				
sample	total	8-MR	12-MR	8-MR/12-MR	FTIR 8-MR/12-MR
HMOR	0.575	0.311	0.264	1.2	1.2
HMOR-TMCS-L	0.427	0.305	0.122	2.5	2.2
HMOR-TMCS-M	0.368	0.296	0.072	4.1	3.6

maximum drop in surface area is only 7% for the HMOR-TMCS-M sample. It is also key to note as well in the pore structure that no change in micro areas and volumes was observed for TMCS-silylated samples in comparison with the parent HMOR zeolite.

Another important consideration is the difference in pore size distributions in the parent and TMCS-silylated HMOR zeolites. The differences in pore size distributions of all samples are shown in Figure 3b, and the micropore size distribution was obtained by a DFT analysis of the N_2 physisorption data. As previously reported in the literature, pores of about 0.67 nm can be assigned to the main channel of 12-MRs and pores of about 0.51 nm correspond to the 8-MR side pockets of HMOR zeolites.[56,57] Obvious information about both 8-MR and 12-MR channels can be observed in all HMOR zeolites, indicating that the pore sizes hardly change during the TMCS-silylation treatment.

Acidic Properties. The most important consideration is whether the TMCS-silylation treatment preferentially removes the BASs within the 12-MR channels of HMOR zeolites, leaving most of the BASs within 8-MR channels. To answer this question, we have quantified the distribution and capacity of the BASs within different channels of HMOR zeolites before and after a TMCS-silylation treatment by ^{1}H MAS NMR spectral analyses of adsorbed pyridine. Pyridine molecules (kinetic diameter 0.58 nm) are mainly absorbed in the 12-MR channels.[12,58] This analysis could help us directly identify the distribution and capacity of BASs within HMOR zeolites, and the corresponding profiles of all samples after exposure to pyridine are illustrated in Figure 4a. Upon chemisorption on HMOR samples, pyridine exhibits unique ^{1}H NMR resonance signals at 15.3 ppm as adsorbing on BASs (i.e., forming a protonic pyridine, PyH^{+}), and the major signals at 3.8 ppm corresponding to the rest of the bridging Si−OH−Al groups (BASs), located in the 8-MR channels of HMOR zeolites, hardly bond with pyridine molecules. The signals at 2.3 and 1.6 ppm can be attributed to extraframework Al−OH and nonacidic Si−OH species, respectively. After pyridine adsorption, the signals of pyridine itself at 6.5−8.3 ppm can also be observed.[18,59] Deconvolution of ^{1}H NMR spectra allows us to quantify the BASs of all HMOR zeolites, and one example of the deconvolution processing of the ^{1}H NMR signals for the HMOR-TMCS-M catalyst is shown in Figure 4b; calculated results of acid sites are given in Table 1. By comparison with the resonance signals of the parent sample at 15.3 and 3.8 ppm, it is found that about 46% of the original BASs are adsorbed by pyridine, located in 12-MR channels, implying that the rest of the BASs (54%) are within the 8-MR channels, which remain inaccessible to pyridine molecules.

From an analysis of NMR spectra, the resonance signals corresponding to protonic pyridine at 15.3 ppm exhibit a dramatic drop with increasing treatment time, indicating that most BASs within the 12-MR channels are removed during the TMCS-silylation treatment. The significant decrease in the number of BASs within the 12-MR channels of HMOR was also evidenced by the decrease in adsorbed pyridine in a Py-TGA analysis (Figure S8) and a reduced cumene conversion in cumene cracking reaction experiments (Figure S9). In contrast, the resonance peaks (3.8 ppm) corresponding to the BASs within the 8-MR channels hardly change for all samples (maximum loss about 4.8%), with very similar intensities, which directly testifies that the acid sites within the 8-MR environments could remain after this treatment. In conjunction with Figure 1a, it could be demonstrated that the loss of BASs within 8-MR channels during the silylation reaction determined by *in situ* DRIFT spectra may be caused by the adsorption of hydrocarbons rather than TMCS molecules, and these BASs are recovered after calcination in the air. What becomes obvious is that, as mentioned above, this TMCS-silylation treatment preferentially and drastically removes the BASs within 12-MR channels and the BASs remain in the 8-MR channels of the HMOR zeolites.

https://doi.org/10.1021/acscatal.1c05896
ACS Catal. 2022, 12, 4491−4500

The significant change in the acid site distribution within the 12- and 8-MR channels is also confirmed by the FTIR spectra (Figure 4c). The spectrum of the parent HMOR shows a highly asymmetric band at 3608 cm^{-1} representing hydroxyl groups. As was mentioned above, this band can be deconvoluted into 3611 and 3592 cm^{-1}, corresponding to the vibration of the Si−OH−Al groups within the 12- and 8-MR channels, respectively. The Si−OH−Al bands in the treated samples became more symmetrical, due to the selective removal of acid sites within 12-MR channels during the TMCS-silylation treatment.

Catalytic Performances for DME Carbonylation. To evaluate the catalytic performances of the parent and TMCS-silylated HMOR catalysts in chemical processes, we consider the carbonylation of DME to MA reaction, which has been proved to be a representative spatially confined reaction on catalytic BASs.[14,60] Figure 5 shows the corresponding DME conversion and MA selectivity of all samples with time on stream (TOS). All HMOR catalysts showed a distinct induction period at the beginning of the reaction. The DME conversion rose rapidly and reached the maximum value as the reaction proceeded. Then, there were distinct differences in the reaction performances of all HMOR catalysts. The DME conversion gradually decreased after reaching the highest value due to coke formation within the 12-MR channels of the untreated sample.[15,61] In the case of TMCS-treated samples, a striking difference is the significantly longer lifetime, especially for the HMOR-TMCS-M catalyst, which has the lowest capacity of acid sites within 12-MR channels in comparison with other samples, which are typically assumed to be responsible for coke formation and catalyst deactivation in the DME carbonylation reaction.[17,19,61]

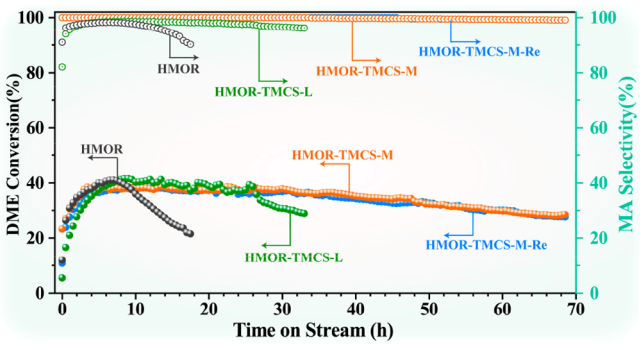

Figure 5. DME carbonylation performances for the untreated and TMCS-silylated HMOR samples. Reaction conditions: 200 °C, 2 MPa, DME/CO/N_2 = 5/35/60, GHSV = 1500 mL/(g h).

Another clear observation in the catalytic performances of all samples is the approximate DME conversion along with TMCS treatment time, due to the similar amounts of acid sites within 8-MR channels determined by ^{1}H MAS NMR spectra. As shown above, these reaction results demonstrate that the preferential removal of the BASs within 12-MR channels to drastically prolong the catalyst service lifetime in DME carbonylation is achieved through the TMCS-silylation treatment.

To investigate the potential regenerability and reusability of TMCS-treated catalysts on the DME carbonylation reaction, the following experiments were conducted. First, the DME carbonylation reaction was routinely run until the HMOR-TMCS-M catalyst was deactivated in the fixed-bed reactor as described above. After this first reaction run, to avoid an artificial loss of catalyst during the regeneration process for the second reaction run, *in situ* regeneration of catalysts (denoted HMOR-TMCS-M-Re) was conducted in the reactor in dry air at 550 °C for 6 h. A comparison of the catalytic performance between the first and second runs is shown in Figure 5. The DME carbonylation performance of the HMOR-TMCS-M catalyst changed little after regeneration and reuse, indicating that the TMCS-modified HMOR zeolites have good regenerability and reusability.

CONCLUSIONS

In summary, the combined use of *in situ* DRIFT and ^{29}Si CP NMR spectroscopic techniques has been employed to investigate the interaction of trimethylchlorosilane (TMCS) molecules with the bridging hydroxyl groups within different positions of the HMOR zeolite. TMCS molecules bridge on the HMOR framework via a hydrolysis reaction between chloro groups and Brønsted H^+ atoms to cover the acid sites. This silylation treatment selectively retains the most of the BASs in the desired position (8-MR environment) by TMCS replacing the Brønsted H^+ atoms within 12-MR channels in the HMOR zeolite, which leads to a better performance in the DME carbonylation reaction. We propose that this modified approach could be further improved by using other silylating agents capable of reacting with the BASs within 12-MR channels, which should be easily diffused through the main 12-MR channels of the HMOR zeolite.

ASSOCIATED CONTENT

Supporting Information

The Supporting Information is available free of charge at https://pubs.acs.org/doi/10.1021/acscatal.1c05896.

Experimental section, online mass spectrometry and gas chromatography results for product distribution during the TMCS-silylation reaction, photos, XRD, N_2 adsorption−desorption data, and SEM of the untreated and various TMCS-silylated HMOR zeolites, TG-DSC curves of HMOR with treatment at 300 °C and MS signals of gaseous thermal decomposition products, cumene catalytic cracking performance of HMOR under different treatment conditions, TG curves and FTIR spectra of all HMOR samples after pyridine adsorption, and ^{29}Si MAS NMR data of HMOR samples (PDF)

AUTHOR INFORMATION

Corresponding Authors

Zhengxi Yu − *National Engineering Laboratory for Methanol to Olefins, Dalian National Laboratory for Clean Energy, Dalian Institute of Chemical Physics, Chinese Academy of Sciences, Dalian 116023, People's Republic of China*; Email: zhengxiyu@dicp.ac.cn

Zhongmin Liu − *National Engineering Laboratory for Methanol to Olefins, Dalian National Laboratory for Clean Energy, Dalian Institute of Chemical Physics, Chinese Academy of Sciences, Dalian 116023, People's Republic of China; University of Chinese Academy of Sciences, Chinese Academy of Sciences, Beijing 100049, People's Republic of China*; orcid.org/0000-0002-7999-2940; Email: liuzm@dicp.ac.cn

https://doi.org/10.1021/acscatal.1c05896
ACS Catal. 2022, 12, 4491−4500

Authors

Rongsheng Liu − *National Engineering Laboratory for Methanol to Olefins, Dalian National Laboratory for Clean Energy, Dalian Institute of Chemical Physics, Chinese Academy of Sciences, Dalian 116023, People's Republic of China; University of Chinese Academy of Sciences, Chinese Academy of Sciences, Beijing 100049, People's Republic of China*

Shu Zeng − *National Engineering Laboratory for Methanol to Olefins, Dalian National Laboratory for Clean Energy, Dalian Institute of Chemical Physics, Chinese Academy of Sciences, Dalian 116023, People's Republic of China; University of Chinese Academy of Sciences, Chinese Academy of Sciences, Beijing 100049, People's Republic of China*

Tantan Sun − *National Engineering Laboratory for Methanol to Olefins, Dalian National Laboratory for Clean Energy, Dalian Institute of Chemical Physics, Chinese Academy of Sciences, Dalian 116023, People's Republic of China*

Shutao Xu − *National Engineering Laboratory for Methanol to Olefins, Dalian National Laboratory for Clean Energy, Dalian Institute of Chemical Physics, Chinese Academy of Sciences, Dalian 116023, People's Republic of China;* orcid.org/0000-0003-4722-8371

Yingxu Wei − *National Engineering Laboratory for Methanol to Olefins, Dalian National Laboratory for Clean Energy, Dalian Institute of Chemical Physics, Chinese Academy of Sciences, Dalian 116023, People's Republic of China*

Complete contact information is available at: https://pubs.acs.org/10.1021/acscatal.1c05896

Notes

The authors declare no competing financial interest.

■ ACKNOWLEDGMENTS

This work was supported by the National Natural Science Foundation of China (Nos. 21991090, 21991093, 21972142, 22022202), the International Partnership Program of the Chinese Academy of Sciences (121421KYSB20180007), and the Key Research Program of Frontier Sciences, CAS (Grant No. QYZDY-SSW-JSC024).

■ REFERENCES

(1) Knott, B. C.; Nimlos, C. T.; Robichaud, D. J.; Nimlos, M. R.; Kim, S.; Gounder, R. Consideration of the Aluminum Distribution in Zeolites in Theoretical and Experimental Catalysis Research. *ACS Catal.* **2018**, *8*, 770−784.

(2) Muraoka, K.; Chaikittisilp, W.; Yanaba, Y.; Yoshikawa, T.; Okubo, T. Directing Aluminum Atoms into Energetically Favorable Tetrahedral Sites in a Zeolite Framework by Using Organic Structure-Directing Agents. *Angew. Chem., Int. Ed.* **2018**, *57*, 3742−3746.

(3) Janda, A.; Vlaisavljevich, B.; Lin, L. C.; Smit, B.; Bell, A. T. Effects of Zeolite Structural Confinement on Adsorption Thermodynamics and Reaction Kinetics for Monomolecular Cracking and Dehydrogenation of n-Butane. *J. Am. Chem. Soc.* **2016**, *138*, 4739−56.

(4) Li, C. G.; Vidal-Moya, A.; Miguel, P. J.; Dedecek, J.; Boronat, M.; Corma, A. Selective Introduction of Acid Sites in Different Confined Positions in ZSM-5 and Its Catalytic Implications. *ACS Catal.* **2018**, *8*, 7688−7697.

(5) Sugi, Y.; Vinu, A. Alkylation of Biphenyl over Zeolites: Shape-Selective Catalysis in Zeolite Channels. *Catalysis Surveys from Asia* **2015**, *19*, 188−200.

(6) Matias, P.; Lopes, J. M.; Laforge, S.; Magnoux, P.; Guisnet, M.; Ramôa Ribeiro, F. n-Heptane transformation over a HMCM-22 zeolite: Catalytic role of the pore systems. *Appl. Catal., A* **2008**, *351*, 174−183.

(7) Huo, H.; Peng, L.; Gan, Z.; Grey, C. P. Solid-state MAS NMR studies of Bronsted acid sites in zeolite H-Mordenite. *J. Am. Chem. Soc.* **2012**, *134*, 9708−20.

(8) Yang, Y. L.; Ding, J. H.; Xu, C. H.; Zhu, W. D.; Wu, P. An insight into crystal morphology-dependent catalytic properties of MOR-type titanosilicate in liquid-phase selective oxidation. *J. Catal.* **2015**, *325*, 101−110.

(9) Gong, K.; Liu, Z.; Liang, L.; Zhao, Z.; Guo, M.; Liu, X.; Han, X.; Bao, X.; Hou, G. Acidity and Local Confinement Effect in Mordenite Probed by Solid-State NMR Spectroscopy. *J. Phys. Chem. Lett.* **2021**, *12*, 2413−2422.

(10) Li, Y.; Huang, S. Y.; Cheng, Z. Z.; Cai, K.; Li, L. D.; Milan, E.; Lv, J.; Wang, Y.; Sun, Q.; Ma, X. B. Promoting the activity of Ce-incorporated MOR in dimethyl ether carbonylation through tailoring the distribution of Bronsted acids. *Appl. Catal., B* **2019**, *256*, 117777.

(11) Zhan, E. S.; Xiong, Z. P.; Shen, W. J. Dimethyl ether carbonylation over zeolites. *J. Energy Chem.* **2019**, *36*, 51−63.

(12) Bhan, A.; Allian, A. D.; Sunley, G. J.; Law, D. J.; Iglesia, E. Specificity of sites within eight-membered ring zeolite channels for carbonylation of methyls to acetyls. *J. Am. Chem. Soc.* **2007**, *129*, 4919−4924.

(13) Cheung, P.; Bhan, A.; Sunley, G. J.; Iglesia, E. Selective carbonylation of dimethyl ether to methyl acetate catalyzed by acidic zeolites. *Angew. Chem., Int. Ed. Engl.* **2006**, *45*, 1617−20.

(14) Boronat, M.; Martinez-Sanchez, C.; Law, D.; Corma, A. Enzyme-like Specificity in Zeolites: A Unique Site Position in Mordenite for Selective Carbonylation of Methanol and Dimethyl Ether with CO. *J. Am. Chem. Soc.* **2008**, *130*, 16316−16323.

(15) Li, B. J.; Xu, J.; Han, B.; Wang, X. M.; Qi, G. D.; Zhang, Z. F.; Wang, C.; Deng, F. Insight into Dimethyl Ether Carbonylation Reaction over Mordenite Zeolite from in-Situ Solid-State NMR Spectroscopy. *J. Phys. Chem. C* **2013**, *117*, 5840−5847.

(16) Liu, Z. Q.; Yi, X. F.; Wang, G. R.; Tang, X. M.; Li, G. C.; Huang, L.; Zheng, A. M. Roles of 8-ring and 12-ring channels in mordenite for carbonylation reaction: From the perspective of molecular adsorption and diffusion. *J. Catal.* **2019**, *369*, 335−344.

(17) Xue, H. F.; Huang, X. M.; Ditzel, E.; Zhan, E. S.; Ma, M.; Shen, W. J. Coking on micrometer- and nanometer-sized mordenite during dimethyl ether carbonylation to methyl acetate. *Chin. J. Catal.* **2013**, *34*, 1496−1503.

(18) He, T.; Liu, X.; Xu, S.; Han, X.; Pan, X.; Hou, G.; Bao, X. Role of 12-Ring Channels of Mordenite in DME Carbonylation Investigated by Solid-State NMR. *J. Phys. Chem. C* **2016**, *120*, 22526.

(19) Cheng, Z. Z.; Huang, S. Y.; Li, Y.; Lv, J.; Cai, K.; Ma, X. B. Deactivation Kinetics for the Carbonylation of Dimethyl Ether to Methyl Acetate on H-MOR. *Ind. Eng. Chem. Res.* **2017**, *56*, 13618−13627.

(20) Li, Y.; Yu, M.; Cai, K.; Wang, M. Y.; Lv, J.; Howe, R. F.; Huang, S. Y.; Ma, X. B. Template-induced Al distribution in MOR and enhanced activity in dimethyl ether carbonylation. *Phys. Chem. Chem. Phys.* **2020**, *22*, 11374−11381.

(21) Zhou, H.; Zhu, W.; Shi, L.; Liu, H.; Liu, S.; Xu, S.; Ni, Y.; Liu, Y.; Li, L.; Liu, Z. Promotion effect of Fe in mordenite zeolite on carbonylation of dimethyl ether to methyl acetate. *Catal. Sci. Technol.* **2015**, *5*, 1961−1968.

(22) Xue, H.; Huang, X.; Zhan, E.; Ma, M.; Shen, W. Selective dealumination of mordenite for enhancing its stability in dimethyl ether carbonylation. *Catal. Commun.* **2013**, *37*, 75−79.

(23) Reule, A. A. C.; Sawada, J. A.; Semagina, N. Effect of selective 4-membered ring dealumination on mordenite-catalyzed dimethyl ether carbonylation. *J. Catal.* **2017**, *349*, 98−109.

(24) Wang, X. S.; Li, R. J.; Yu, C. C.; Liu, Y. X.; Zhang, L. Y.; Xu, C. M.; Zhou, H. J. Enhancing the dimethyl ether carbonylation performance over mordenite catalysts by simple alkaline treatment. *Fuel* **2019**, *239*, 794−803.

(25) Liu, S. P.; Fang, X. D.; Liu, Y.; Liu, H. C.; Ma, X. G.; Zhu, W. L.; Liu, Z. M. Dimethyl ether Carbonylation over Mordenite zeolite

modified by Alkyimidazolium ions. *Catal. Commun.* **2020**, *147*, 106161.
(26) Cao, K. P.; Fan, D.; Li, L. Y.; Fan, B. H.; Wang, L. Y.; Zhu, D. L.; Wang, Q. Y.; Tian, P.; Liu, Z. M. Insights into the Pyridine-Modified MOR Zeolite Catalysts for DME Carbonylation. *ACS Catal.* **2020**, *10*, 3372−3380.
(27) Liu, J.; Xue, H.; Huang, X.; Wu, P.-H.; Huang, S.-J.; Liu, S.-B.; Shen, W. Stability Enhancement of H-Mordenite in Dimethyl Ether Carbonylation to Methyl Acetate by Pre-adsorption of Pyridine. *Chin. J. Catal.* **2010**, *31*, 729−738.
(28) Li, Y.; Sun, Q.; Huang, S. Y.; Cheng, Z. Z.; Cai, K.; Lv, J.; Ma, X. B. Dimethyl ether carbonylation over pyridine-modified MOR: Enhanced stability influenced by acidity. *Catal. Today* **2018**, *311*, 81−88.
(29) Weber, R.W; Moller, K.P; Unger, M; O'Connor, C.T The chemical vapour and liquid deposition of tetraethoxysilane on the external surface of ZSM-5. *Microporous Mesoporous Mater.* **1998**, *23*, 179−187.
(30) Weber, R.W.; Moller, K.P.; O'Connor, C.T. The chemical vapour and liquid deposition of tetraethoxysilane on ZSM-5, mordenite and beta. *Microporous Mesoporous Mater.* **2000**, *35-36*, 533−543.
(31) Akiyama, S.; Mochizuki, H.; Yamazaki, H.; Yokoi, T.; Tatsumi, T.; Kondo, J. N. The effective silylation of external surface on H-ZSM5 with cyclic siloxane for the catalytic cracking of naphtha. *Mol. Catal.* **2017**, *433*, 48−54.
(32) Tempelman, C. H. L.; de Rodrigues, V. O.; van Eck, E. R. H.; Magusin, P.; Hensen, E. J. M. Desilication and silylation of Mo/HZSM-5 for methane dehydroaromatization. *Microporous Mesoporous Mater.* **2015**, *203*, 259−273.
(33) Zhu, Z.; Xie, Z.; Chen, Q.; Kong, D.; Li, W.; Yang, W.; Li, C. Chemical liquid deposition with polysiloxane of ZSM-5 and its effect on acidity and catalytic properties. *Microporous Mesoporous Mater.* **2007**, *101*, 169−175.
(34) Ding, W.; Meitzner, G. D.; Iglesia, E. The Effects of Silanation of External Acid Sites on the Structure and Catalytic Behavior of Mo/H−ZSM5. *J. Catal.* **2002**, *206*, 14−22.
(35) McAteer, J. C.; Rooney, J. J. Modification of HY zeolite by reaction with tetramethylsilane. *Adv. Chem. Ser.* **1973**, *121*, 258−266.
(36) Barrer, R. M.; Jenkins, R. G.; Peeters, G. Silanation of Zeolites. In *Molecular Sieves—II*; American Chemical Society: 1977; Vol. *40*, pp 258−270.
(37) Barrer, R. M.; Vansant, E. F.; Peeters, G. Sorption behavior of silanated H-mordenite. *J. Chem. Soc.-Faraday Transactions I* **1978**, *74*, 1871−1878.
(38) Prodinger, S.; Derewinski, M. A.; Vjunov, A.; Burton, S. D.; Arslan, I.; Lercher, J. A. Improving Stability of Zeolites in Aqueous Phase via Selective Removal of Structural Defects. *J. Am. Chem. Soc.* **2016**, *138*, 4408−4415.
(39) Hara, K.; Akahane, S.; Wiench, J. W.; Burgin, B. R.; Ishito, N.; Lin, V. S. Y.; Fukuoka, A.; Pruski, M. Selective and Efficient Silylation of Mesoporous Silica: A Quantitative Assessment of Synthetic Strategies by Solid-State NMR. *J. Phys. Chem. C* **2012**, *116*, 7083−7090.
(40) Osuga, R.; Yokoi, T.; Doitomi, K.; Hirao, H.; Kondo, J. N. Infrared Investigation of Dynamic Behavior of Bronsted Acid Sites on Zeolites at High Temperatures. *J. Phys. Chem. C* **2017**, *121*, 25411−25420.
(41) Zhou, H.; Zhu, W. L.; Shi, L.; Liu, H. C.; Liu, S. P.; Ni, Y. M.; Liu, Y.; He, Y. L.; Xu, S. L.; Li, L. N.; Liu, Z. M. In situ DRIFT study of dimethyl ether carbonylation to methyl acetate on H-mordenite. *J. Mol. Catal. a-Chem.* **2016**, *417*, 1−9.
(42) Prodinger, S.; Shi, H.; Eckstein, S.; Hu, J. Z.; Olarte, M. V.; Camaioni, D. M.; Derewinski, M. A.; Lercher, J. A. Stability of Zeolites in Aqueous Phase Reactions. *Chem. Mater.* **2017**, *29*, 7255−7262.
(43) Zapata, P. A.; Faria, J.; Ruiz, M. P.; Jentoft, R. E.; Resasco, D. E. Hydrophobic Zeolites for Biofuel Upgrading Reactions at the Liquid−Liquid Interface in Water/Oil Emulsions. *J. Am. Chem. Soc.* **2012**, *134*, 8570−8578.
(44) Mirji, S. A.; Halligudi, S. B.; Sawant, D. P.; Jacob, N. E.; Patil, K. R.; Gaikwad, A. B.; Pradhan, S. D. Adsorption of octadecyltrichlorosilane on mesoporous SBA-15. *Appl. Surf. Sci.* **2006**, *252*, 4097−4103.
(45) Wang, X. S.; Li, R. J.; Yu, C. C.; Liu, Y. X.; Liu, L. M.; Xu, C. M.; Zhou, H. J.; Lu, C. X. Influence of Acid Site Distribution on Dimethyl Ether Carbonylation over Mordenite. *Ind. Eng. Chem. Res.* **2019**, *58*, 18065−18072.
(46) Tian, P.; Wei, Y.; Ye, M.; Liu, Z. Methanol to Olefins (MTO): From Fundamentals to Commercialization. *ACS Catal.* **2015**, *5*, 1922−1938.
(47) Qi, L.; Wei, Y. X.; Xu, L.; Liu, Z. M. Reaction Behaviors and Kinetics during Induction Period of Methanol Conversion on HZSM-5 Zeolite. *ACS Catal.* **2015**, *5*, 3973−3982.
(48) Wei, Y. X.; Zhang, D. Z.; Chang, F. X.; Xia, Q. H.; Su, B. L.; Liu, Z. M. Ultra-short contact time conversion of chloromethane to olefins over pre-coked SAPO-34: direct insight into the primary conversion with coke deposition. *Chem. Commun.* **2009**, 5999−6001.
(49) Fyfe, C. A.; Gobbi, G. C.; Kennedy, G. J. Quantitatively reliable Si-29 magic-angle spinning nuclear magnetic-resonance spectra of surfaces and surface-immobilized species at high-field using a conventional high-resolution spectrometer. *J. Phys. Chem.* **1985**, *89*, 277−281.
(50) Iyoki, K.; Kikumasa, K.; Onishi, T.; Yonezawa, Y.; Chokkalingam, A.; Yanaba, Y.; Matsumoto, T.; Osuga, R.; Elangovan, S. P.; Kondo, J. N.; Endo, A.; Okubo, T.; Wakihara, T. Extremely Stable Zeolites Developed via Designed Liquid-Mediated Treatment. *J. Am. Chem. Soc.* **2020**, *142*, 3931−3938.
(51) Kraushaar, B.; Van De Ven, L. J. M.; De Haan, J. W.; Van Hooff, J. H. C.; Grobet, P. J.; Mortier, W. J.; Vansant, E. F.; Schulz-Ekloff, G. Clusters of Terminal Groups in ZSM-5: A Study Performed by Silylation and 29Si CP MAS NMR. *Stud. Surf. Sci. Catal.* **1988**, *37*, 167−174.
(52) Bein, T.; Carver, R. F.; Farlee, R. D.; Stucky, G. D. Solid-state Si-29 NMR and infrared studies of the reactions of monofunctional and polyfunctional silanes with zeolite-Y surfaces. *J. Am. Chem. Soc.* **1988**, *110*, 4546−4553.
(53) Ma, Z. P.; Xie, J. Y.; Zhang, J. L.; Zhang, W.; Zhou, Y.; Wang, J. Mordenite zeolite with ultrahigh SiO2/Al2O3 ratio directly synthesized from ionic liquid-assisted dry-gel-conversion. *Microporous Mesoporous Mater.* **2016**, *224*, 17−25.
(54) Muller, M.; Harvey, G.; Prins, R. Comparison of the dealumination of zeolites beta, mordenite, ZSM-5 and ferrierite by thermal treatment, leaching with oxalic acid and treatment with SiCl4 by H-1, Si-29 and Al-27 MAS NMR. *Microporous Mesoporous Mater.* **2000**, *34*, 135−147.
(55) Koranyi, T. I.; Nagy, J. B. Distribution of aluminum in different periodical building units of MOR and BEA zeolites. *J. Phys. Chem. B* **2005**, *109*, 15791−15797.
(56) Reule, A. A. C.; Prasad, V.; Semagina, N. Effect of Cu and Zn ion-exchange locations on mordenite performance in dimethyl ether carbonylation. *Microporous Mesoporous Mater.* **2018**, *263*, 220−230.
(57) Ban, S.; van Laak, A. N. C.; Landers, J.; Neimark, A. V.; de Jongh, P. E.; de Jong, K. P.; Vlugt, T. J. H. Insight into the Effect of Dealumination on Mordenite Using Experimentally Validated Simulations. *J. Phys. Chem. C* **2010**, *114*, 2056−2065.
(58) Maache, M.; Janin, A.; Lavalley, J. C.; Benazzi, E. FT infrared study of Brønsted acidity of H-mordenites: Heterogeneity and effect of dealumination. *Zeolites* **1995**, *15*, 507−516.
(59) Haase, F.; Sauer, J. Interaction of methanol with bronsted acid sites of zeolite catalysts-An-ab-initio study. *J. Am. Chem. Soc.* **1995**, *117*, 3780−3789.
(60) Chu, Y. Y.; Lo, A. Y.; Wang, C.; Deng, F. Origin of High Selectivity of Dimethyl Ether Carbonylation in the 8-Membered Ring Channel of Mordenite Zeolite. *J. Phys. Chem. C* **2019**, *123*, 15503−15512.

https://doi.org/10.1021/acscatal.1c05896
ACS Catal. 2022, 12, 4491−4500

(61) Xue, H. F.; Huang, X. M.; Ditzel, E.; Zhan, E. S.; Ma, M.; Shen, W. J. Dimethyl Ether Carbonylation to Methyl Acetate over Nanosized Mordenites. *Ind. Eng. Chem. Res.* **2013**, *52*, 11510−11515.

https://doi.org/10.1021/acscatal.1c05896
ACS Catal. 2022, 12, 4491−4500